Estimation of the IC to CG Ratio Using JEM-GLIMS and Ground-based Lightning Network Data

K. Bandholnopparat[1*], M. Sato[2], T. Adachi[3], T. Ushio[4], and Y. Takahashi[2]

[1] Department of Cosmosciences, Hokkaido University, Sapporo, Japan.

[2] Faculty of Science, Hokkaido University, Sapporo, Japan.

[3] Meteorological Research Institute, Tsukuba, Japan.

[4] Department of Aerospace Engineering, Tokyo Metropolitan University, Hino, Japan.

Corresponding author: Kittanapat Bandholnopparat (kbjack@ep.sci.hokudai.ac.jp)

Department of Cosmosciences, Hokkaido University, Kita-10 Nishi-8, Kita-ku, Sapporo, 060-0810, JAPAN

Key Points:

A new method for classifying the lightning discharge type has been developed using JEM-GLIMS and the ground-based lightning data.

The observations using JEM-GLIMS and ground-based lightning detection networks were used to study the geographic distribution of Z-ratio.

The strong relationship between Z-ratio and latitude was found, in which, it has a good agreement compared with previous studies.

Abstract

The occurrence ratio of intracloud (IC) to cloud-to-ground (CG) discharges, which is denoted by *Z*-ratio, is the crucial parameter for the studies on the climatological differences of thunderstorm structures and the quantitative evaluation of lightning contributions to the global electric circuit. However, the latitudinal, regional, and seasonal dependences of *Z*-ratio are not fully clarified. Therefore, using optical data obtained by the JEM-GLIMS mission, we distinguished the lightning discharge type, *i.e.*, IC, positive CG (+CG), and negative CG (-CG) discharges, and statistically estimated the Z-ratio. We analyzed 8354 JEM-GLIMS lightning events and succeeded in identifying 4431 IC discharges, 597 +CG discharges, and 3326 -CG discharges. From this result, we calculated the *Z*-ratio and estimated its latitudinal, regional, and seasonal dependences. It is found that the *Z*-ratio is slightly higher over the continental area than the oceanic area. In addition, the average *Z*-ratio in the local summer season is higher than that in the local winter season. The clear latitudinal dependence of the *Z*-ratio is also found, which is generally comparable to the results shown in the previous studies. The estimated *Z*-ratio varies from 2.9 - 0.19 from the equator to 50° latitude, and the global mean value is 1.6. The regional dependence of *Z*-ratio derived from this study can be combined with the CG lightning data provided by the ground-based lightning detection networks to estimate the occurrence number of IC discharges. It will greatly contribute to a more accurate estimation of the total lightning currents in the global electric circuit.

1. Introduction

The occurrence ratio of intracloud (IC) to cloud-to-ground (CG) discharges is reflected by the fundamental aspects of lightning activities. Usually, this ratio is denoted by $Z = N_{IC}/N_{CG}$, where N_{IC} and N_{CG} are the occurrence number of IC and CG discharges, respectively. The *Z*-ratio is essentially important from several standpoints: (i) to evaluate regional or global NO_x production by lightning (Pickering et al., 1998; Rakov and Uman, 2003; Ott et al., 2010), (ii) to estimate the contribution of lightning discharges to the global electrical circuit (Williams, 2009; Rycroft and Odzimek, 2010; Mareev and Volodin, 2014), (iii) to study kinematics and microphysics of thunderstorms (Williams et al., 1999; Buechler et al., 2000), and so on. The latitudinal dependence of the *Z*-ratio was firstly reported by Pierce (1970). It was found that the

Z-ratio decreases according to the increase of latitude. Prentice and Mackerras (1977) analyzed lightning data obtained from 29 ground-based stations at different locations around the globe to study the relationship between *Z*-ratios and latitude, and they confirmed the *Z*-ratio decreases from the equator to the mid-latitudes with the value ranging from 9.0 to 1.5.

The satellite-based observations such as the Optical Transient Detector (OTD) and the Lightning Images Sensor (LIS) (Boccippio et al., 2000; Christian et al., 2003; Koshak, 2010) have made us possible to observe lightning discharges (both IC and CG discharges) over wider regions and long periods with the high detection efficiency. Boccippio et al. (2001) used OTD data obtained during the four years observation period and the ground-based lightning data obtained by the National Lightning Detection Network (NLDN) to determine the geographical distribution of lightning flashes and *Z*-ratios over the United States. The large range of *Z*-ratios was found in the regions where the occurrence rates of +CG discharges and severe storms are high. They also investigated the dependence of *Z*-ratios on latitude, longitude, and orographic effects. However, they did not find out the apparent geographical dependence of the *Z*-ratio. Although they found the low *Z*-ratio values in mountain regions, it does not seem to be unique and is hard to conclude that this relation is linked with orographic effects or meteorological effects. They suggested that the intensity, morphology and/or level of organization of thunderstorms have more significant impacts on the *Z*-ratios than the environmental factors such as the freezing level altitude, tropospheric depth or surface elevation. Kuleshov et al. (2006) analyzed the ground-based lightning data obtained by the lightning flash counters (CIGRE-500 and CGR3) and the satellite-based lightning data obtained by the OTD and LIS in order to estimate *Z*-ratios over Australia using the same methodology as Boccippio et al. (2001). They found that the *Z*-ratios ranged from 0.75 to 7.7 and concluded that the most representative *Z*-ratio is ~2 ± 30% in the latitudinal range of Australia and that there is not clear latitudinal dependence. Soriano and de Pablo (2007) also analyzed both the satellite-based lightning data obtained by the OTD and the ground-based lightning data obtained by the Spanish lightning detection networks to estimate *Z*-ratios over the Iberian Peninsula (35ºN - 44ºN). It is found that the estimated *Z*-ratio decreased according to the increase of latitude. It is also found that the *Z*-ratios ranged from 2.2 to 6.0 and that the spatial and annual average of the *Z*-ratio in this latitudinal range was 3.48. de Souza et al. (2009) analyzed the OTD data and the ground-based lightning data from the Brazilian Lightning Detection Network (BrazilDat) and estimated *Z*-ratios over the southern part of Brazil (14ºS - 25ºS). They reported that the latitudinal dependence of the *Z*-ratios was not confirmed in this area and that there was no clear relation between the *Z*-ratios and the population of +CG discharges.

Although the lightning data obtained by the space-borne and ground-based observations were analyzed in the previous studies in order to clarify the geographical distribution of *Z*-ratios, these studies focused on only a specific and limited area where the ground-based lightning data was available. Therefore, the regional, latitudinal, and seasonal variations of *Z*-ratios in the global scale are not fully understood yet. In this study, we analyzed 8354 lightning events measured by the Global Lightning and Sprite Measurements on Japanese Experiment Module (JEM-GLIMS) mission onboard the International Space Station (ISS) in order to estimate the regional, latitudinal, and seasonal variation of *Z*-ratios. In section 2, the methodology to categorize the lightning discharge type using both JEM-GLIMS data and ground-based lightning data is introduced. The results of the calculated *Z*-ratios are presented in section 3. The latitudinal, seasonal, and regional variations of *Z*-ratios are also shown in this section. Finally, the discussion and conclusions of this study are presented in section 4.

2. Method

In order to study the latitudinal, regional, and seasonal variations of Z-ratios, we analyzed 8354 lightning events detected by the JEM-GLIMS optical instruments between November 2012 and August 2015. These lightning events were detected over both oceanic and continental regions and from 51ºS to 51ºN as shown in Figure 1. Note that, the gray hatched areas in Figure 1 are the region where JEM-GLIMS did not conduct the observations because of the limitation of the orbital inclination angle of the ISS. The JEM-GLIMS optical instruments were designed to measure the optical emissions of lightning and transient luminous events (TLEs) in the nadir direction form the ISS (Ushio et al., 2014; Sato et al., 2015). They consist of the six-channel spectrophotometers (PHs) and the Lightning and Sprite Imager (LSI). The PHs measure absolute optical intensity of lightning discharges in the wavelength range of 150-280 nm (PH1), 310-321 nm (PH5), 332-342 nm (PH2), 386-397 nm (PH6), 599-900 nm (PH4), 755-766 nm (PH3), respectively (Sato et al, 2011a, 2015, 2016; Adachi et al., 2016). The LSI consists of two CMOS cameras: (1) the wind-band CMOS camera (LSI-1) with 768-830 nm optical filter, and (2) the narrowband CMOS camera (LSI-2) with 760-775 nm filter (Sato et al., 2011b, 2015, 2016). These cameras are dedicated to measuring the optical shape of the lightning and TLE emissions. More information on the specifications and the operation of the JEM-GLIMS instruments can be found in the papers of Ushio et al. (2014), Sato et al. (2015, 2016), and Adachi et al. (2016).

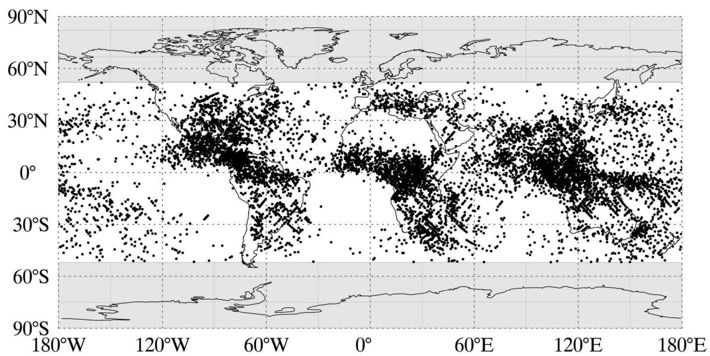

Figure 1. The global distribution of the 8354 lightning events detected by JEM-GLIMS between November 2012 and August 2015 and used in this study to estimate the *Z*-ratios.

The flow chart showing how we identified the IC discharge and CG discharge of JEM-GLIMS lightning events using the ground-based lightning network, *i.e.*, the Japanese Lightning Detection Network (JLDN), the World Wide Lightning Location Network (WWLLN), the Global ELF Observation Network (GEON), and the NLDN is summarized in Figure 2. The full details of the methods used can be found in our previous paper (Bandholnopparat et al., 2017, 2019). In brief, Firstly, we compared JEM-GLIMS data to the ground-based lightning data to identify discharge types of JEM-GLIMS lightning events, *i.e.*, IC discharge and CG discharge. Then, we further analyzed the ELF magnetic field waveform data detected by the GEON and estimated the polarity of CG discharges, *i.e.,* +CG or -CG, using the magnetic direction finding method, which is introduced by Sato et al. (2003).

By comparing JEM-GLIMS lightning data and the ground-based lightning data, we succeeded in identifying the discharge type of 571 JEM-GLIMS lightning events. It was found that 75, 102, and 394 events were determined to be IC, +CG, and -CG discharges, respectively. However, we could not succeed in classifying the discharge type of 6532 JEM-GLIMS lightning events. One reason is the limitation of the area where we can compare JEM-GLIMS lightning data to NLDN and JLDN data, *i.e.,* the continents of North A er is the low detection efficiency of the WWLLN, though it covers wh 006, 2009; Hutchins et al., 2012). Therefore, in order to identify the discharge type of both 6532 ambiguous lightning events and 1251 CG events, we applied new criteria, which is the intensity ratio between blue and red emissions measured by PHs, *i.e.*, PH2/PH3, PH5/PH3, PH6/PH3, PH2/PH4, PH5/PH4, and PH6/PH4 as the indicator of the discharge types. This method is based on the different height of lightning discharge channels and the different attenuation rate of blue and red emissions from lightning discharge channels to the ISS. Blue emissions from lightning discharges (*i.e.*, 310-321 nm, 332-342 nm, 386-397 nm) are more absorbed and attenuated than red emissions (*i.e.*, 755-766 nm, 599-900 nm). IC and +CG discharge channels tend to locate at the higher altitude than -CG discharge channels (Mackerras, 1968; Ballarotti et al., 2005; Stolzenburg et al., 2013; Lopez et al., 2016; Sun et al., 2016; Lyu et al., 2016). Consequently, red emissions from -CG discharges mainly reach to the JEM-GLIMS optical instruments. On the other hand, IC discharge channels are located between the main positive charge region and the main negative charge region (Mecikalski and Carey, 2018), and +CG discharge channels are located between the main positive charge region and the ground. Hence, both red and blue emissions reach to the JEM-GLIMS optical instruments. Then, the ratio between blue to the red emissions of IC and +CG discharges might be higher than that of -CG discharges.

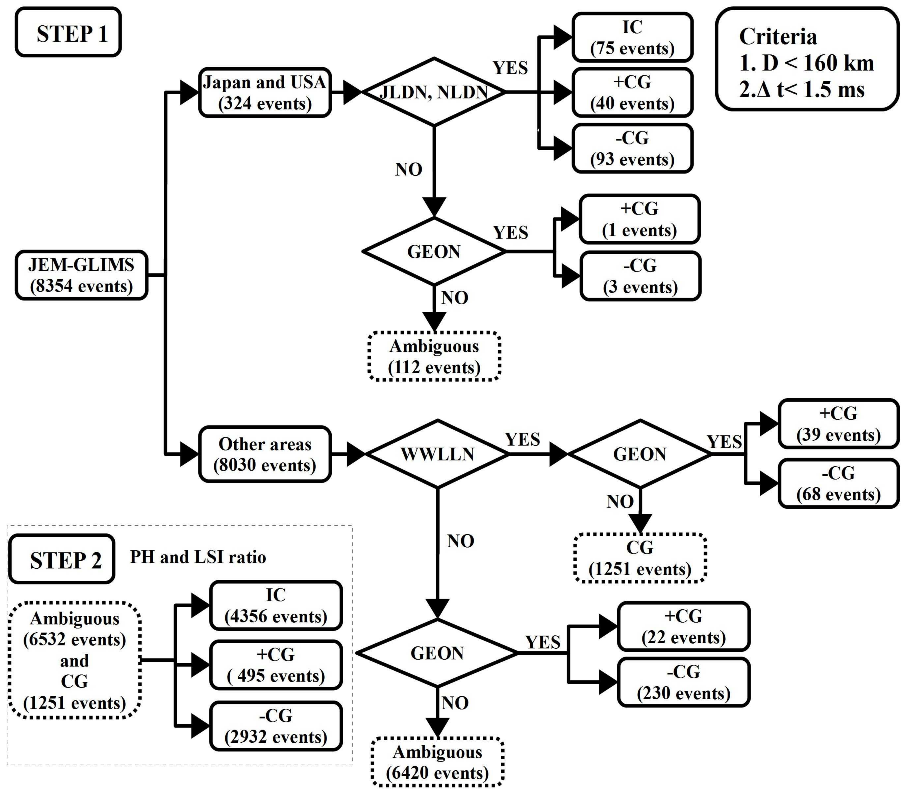

Figure 2. Flow chart showing how the discharge type of the JEM-GLIMS lightning events were categorized into "IC discharge", "-CG discharge", "+CG discharge", "CG discharge (unknown polarity)", and "ambiguous discharge events" using the ground-based lightning data provided by JLDN, NLDN, WWLLN, and GEON.

As a next step, the number of lightning events detected by JEM-GLIMS was counted at each 3.0º × 3.0º grid, which contains the FOV of PHs at the equator. Then, the ratio of IC to CG discharges (*Z*-ratio) at each grid was calculated according to the following formula,

$$Z = \frac{\left(\frac{N_{IC}}{DE_{IC}}\right)}{\left(\frac{N_{-CG}}{DE_{-CG}}\right) + \left(\frac{N_{+CG}}{DE_{+CG}}\right)} \qquad (1)$$

where N_{IC}, N_{+CG}, and N_{-CG} are the number of IC, +CG, and -CG discharge events, and DE_{IC}, DE_{+CG}, and DE_{-CG} are the detection efficiency of IC, +CG, and -CG discharges, respectively. The

JEM-GLIMS detection efficiency of IC, +CG, and -CG discharges are estimated to be 11.2%, 28.3%, and 19.7%, respectively. The detailed estimation method of these detection efficiency is presented at appendix A.

3. Results and Discussion

3.1 PH and LSI intensity ratios of IC, +CG, and -CG discharges

The histogram of the PH intensity ratios, *i.e.*, PH2/PH3, PH5/PH3, PH6/PH3, PH2/PH4, PH5/PH4, and PH6/PH4, of the identified 75 IC, 102 +CG, and 394 -CG discharges are shown in Figure 3. In this figure, the PH intensity ratios are indicated by the logarithmic values at the horizontal axis. The median value of the logarithmic PH intensity ratios and the standard deviation (σ) are also summarized in Table 1. As shown in Table 1, it is found that the PH intensity ratio of the IC discharges is the highest in all lightning types. It is also found that the PH intensity ratio of the -CG discharges is always the smallest while those of +CG discharges are larger than those of the -CG discharges but smaller than those of the IC discharges, whereas Bandholnopparat et al. (2019) found that the PH intensity ratio of +CG is the highest, and they also found that the PH intensity ratio of the -CG discharges is always the smallest while those of IC discharges are larger than those of the -CG discharges but smaller than those of the +CG discharges. The primary cause of the discrepancy is due to the +CG discharges which initiate from the lower positive charge region (LPCR). Although the normal arc-type discharge channels of +CG discharges tend to occur at a higher altitude between the main positive charge region near the cloud top and the ground (Rust et al., 1981; Lu et al., 2012), some +CG discharges arise from the LPCR in the thundercloud (Pawar and Kamra, 2004). The discharge channel of these +CG discharges locates between LPCR near the cloud bottom and the ground. Consequently, the median PH intensity ratios of +CG discharges in Table 1 are between IC and -CG discharges in all lightning types.

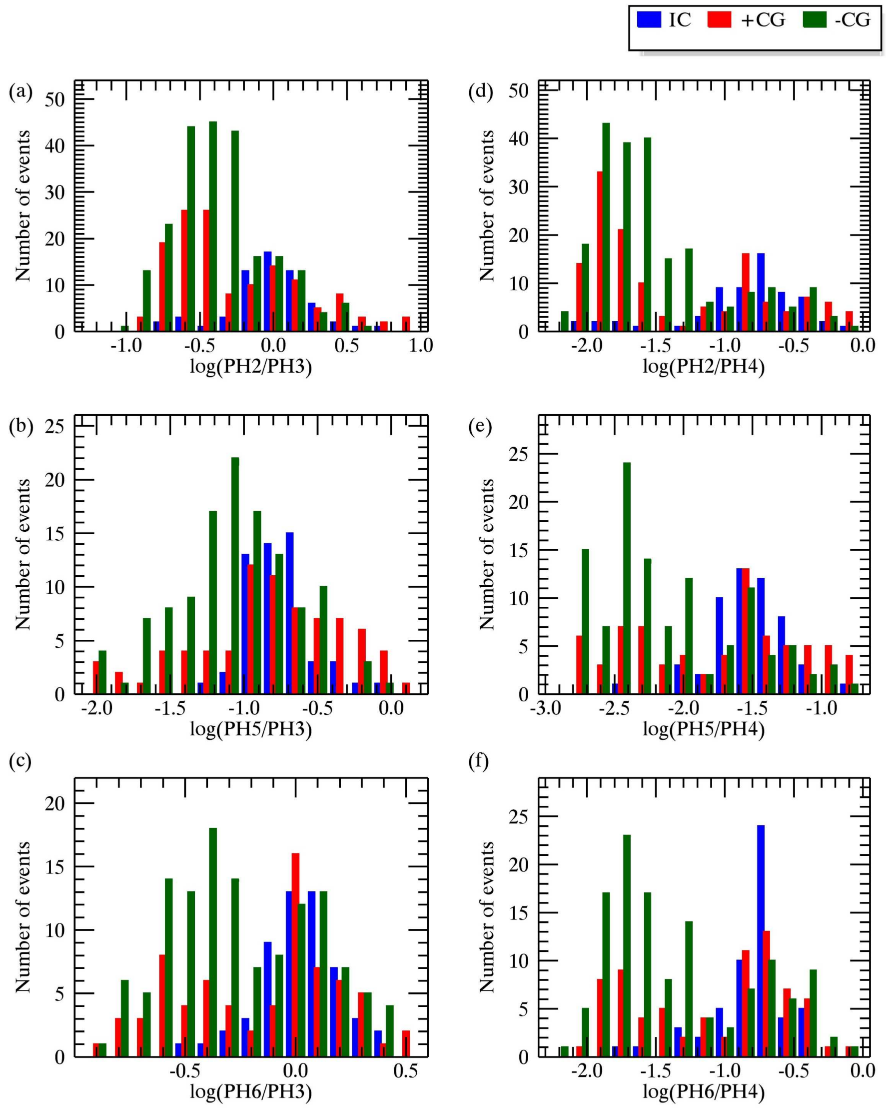

Figure 3. Histograms of the PH intensity ratios with the logarithmic scale. The blue, red and green bars correspond to the ratio of IC, +CG, and -CG discharges, respectively. (a)-(f) are the ratios of PH2/PH3, PH5/PH3, PH6/PH3, PH2/PH4, PH5/PH4, and PH6/PH4, respectively.

The LSI intensity ratios of the identified lightning discharge events were also calculated, and the histogram of the calculated LSI intensity ratios is shown in Figure 4. The median value and standard deviation are also presented in this figure. The number of the lightning events used for the LSI intensity ratio calculation is smaller than that for the PH intensity ratio calculation analysis because the LSI-2 could detect lightning optical emissions only in 107 from 521 lightning events. This is because the lightning emissions in 762 nm were severely absorbed by the atmospheric oxygen molecules. As shown in Figure 4, the median values of IC, +CG and -CG discharges were estimated to be 0.063, 0.049, and 0.038, respectively. It is clear that the characteristics of the LSI intensity ratios are in good agreement with the result of PH intensity ratios.

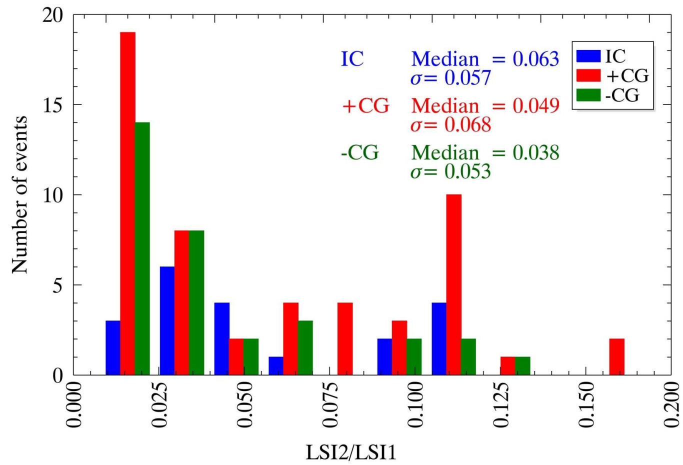

Figure 4. Histograms of the LSI intensity ratio of 45 IC (blue), 12 +CG (red), and 17 -CG (green) discharges. The median value and the standard deviation of the LSI intensity ratio of each lightning type are also indicated in this figure.

Table 1. Summary of the PH and LSI intensity ratios of 75 IC, 102 +CG, and 394 -CG discharges. In this table, the median value of the logarithmic PH and LSI intensity ratios and the standard deviation (σ) are listed.

	+CG		IC		-CG	
	median	σ_{+CG}	median	σ_{IC}	median	σ_{-CG}
log(PH2/PH3)	-0.33	0.48	0.097	0.32	-0.36	0.32
log(PH5/PH3)	-0.72	0.57	-0.62	0.23	-1.0	0.46
log(PH6/PH3)	0.019	0.38	0.099	0.17	-0.27	0.36
log(PH2/PH4)	-1.5	0.67	-0.71	0.48	-1.6	0.49
log(PH5/PH4)	-1.5	0.68	-1.44	0.28	-2.2	0.55
log(PH6/PH4)	-0.79	0.55	-0.68	0.29	-1.5	0.54

As shown in Figures 3 and 4 and Table 1, the distribution of PH and LSI intensity ratios of the IC, +CG, and -CG discharges show the clear difference. Therefore, we can conclude that these PH and LSI intensity ratios are useful indicators for distinguishing the discharge type of other 7783 JEM-GLIMS lightning events.

3.2 Regional Dependence of *Z*-ratio

Figures 5(a)-5(c) show the global distribution of the identified IC, +CG, and -CG discharges measured by JEM-GLIMS. In order to estimate regional dependences of the *Z*-ratio, the lightning detection numbers in each 3.0º × 3.0º grid are counted, and the *Z*-ratio was calculated every grid. The spatial distribution of the *Z*-ratio is shown in Figure 6. It is found that the *Z*-ratio varies from 0.2 to 17.1 and that the average value is 1.6, though Mackerras and Darveniza (1994) estimated the mean *Z*-ratio to be 1.9 from the analysis of the lightning data obtained by the fourteen CGR3 counters. Interestingly, our result also shows that the higher *Z*-ratio tends to occur over the continental region than the oceanic region. Especially, the *Z*-ratio tends to be high near the equator. The average *Z*-ratio over the continental and oceanic areas is 1.7 and 1.1, respectively. It should be noted that the definition of the continental and oceanic areas used in this study is the same as that introduced by Mackerras et al. (1998). The possible explanation for this finding may be that the thundercloud structure and the electrical charge distributions in the thunderclouds are different in the continental and oceanic thunderclouds. It was reported that the lightning occurrence frequency is related to the strong upward velocity in thunderclouds and the convective available potential energy (CAPE) (Lhermitte and Williams, 1983). It was found that the high CAPE values are usually observed in the continental air masses, while the low CAPE values are usually observed in the oceanic air masses. This causes the weaker updrafts in the oceanic thunderclouds than the continental thunderclouds (Zipser, 1994; Zipser and Lutz, 1994). The weaker updrafts in the oceanic thunderclouds cause a less efficient charge separations (Takahashi, 1984; Ziegler et al., 1991; Norville et al.,1991; Stolzenburg et al., 1998a, 1998b, 1998c). Thus, the main negative charge region inside the oceanic thunderclouds tends to locate at the lower altitude than that inside the continental thunderclouds, which enhances the occurrence rate of CG discharges. However, this hypothesis needs to be verified in a future study.It should be noted that the continental and oceanic areas used in this study is the same definition as that introduced by Mackerras et al. (1998).

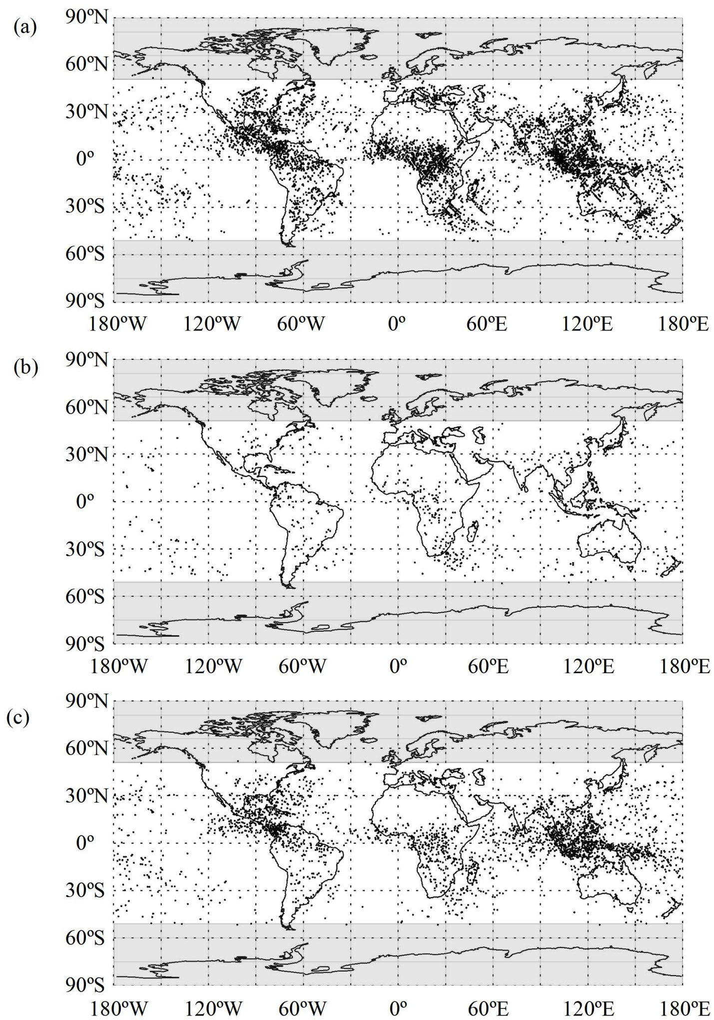

Figure 5. The global distribution of the identified (a) IC discharges, (b) +CG discharges, and (c) -CG discharges detected by JEM-GLIMS in the period from November 2012 – August 2015.

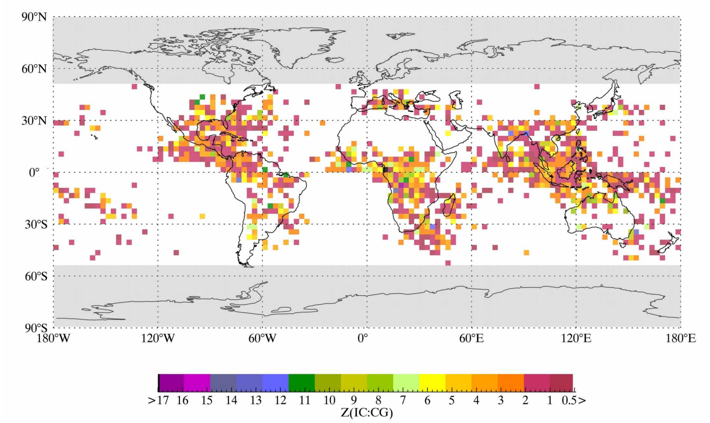

Figure 6. Spatial distribution of the *Z*-ratio over the latitudinal range of ±51°.

3.3 Seasonal dependence

Figures 7(a)-7(d) show the global map of the *Z*-ratio in the period of December - February, March - May, June - August, and September - November, respectively. In the period of December - February, the pixels where the *Z*-ratio exists can be found mainly in the southern hemisphere, especially, between the equator to 30°S, as shown in Figure 7(a). While, in the period from June - August, these pixels can be found mainly in the northern hemisphere between the equator to 30°N, as shown in Figure 7(c). However, the distribution of those pixels in the period of March - May and September - November can be found both in the northern and southern hemispheres, and they are mainly located in the latitudinal range of 30°S – 30°N, as shown in Figures 7(b) and 7(c). It is found that in the northern tropics (from 0° to 20° N) the average *Z*-ratio value in the local summer season (June - August) is 2.4 times higher than that in the local winter season (December - February). Similarly, it is found that in the southern tropics (0° to 20° S) the average *Z*-ratio value in the local summer season (December - February) is 2.3 times higher than that in the local winter season (June - August). In contrast, the averaged *Z*-ratio values in the northern and southern hemispheres in the period of March - May are almost comparable to those in the period of September - November.

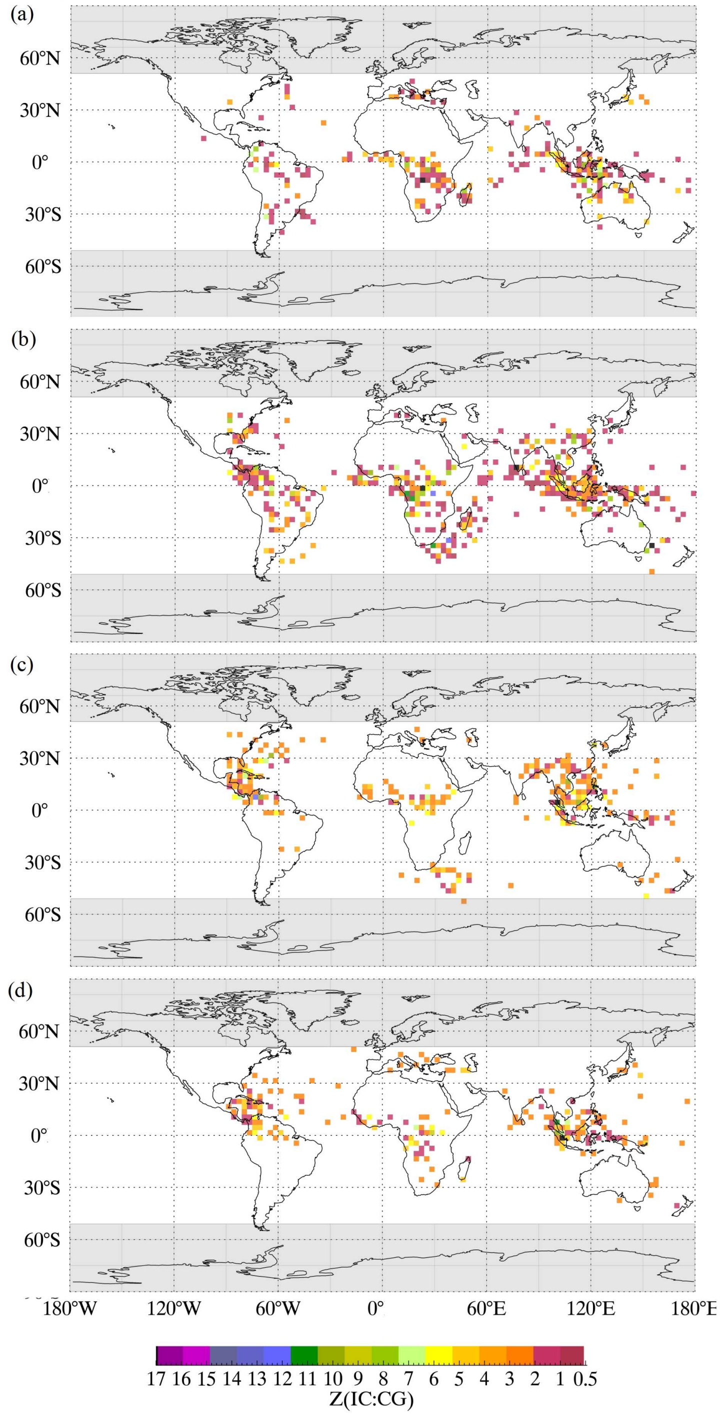

Figure 7. Spatial distribution of the *Z*-ratio in the period of (a) December-February, (b) March-May, (c) June-August, and (d) September-November, respectively.

A possible explanation for the difference of the *Z*-ratio values in the local summer/winter seasons may be related to the altitude difference of the main negative charge region in the thunderclouds. As we describe in Section 3.1, the height of the main negative charge region in thunderclouds is the function of the freezing levels and CAPE. In the local summer season, the ground temperature is higher compared to the local winter season. Consequently, the main negative charge region tends to locate at the higher altitude and tend to be closer to the main positive charge region. The smaller distance between the main positive and negative charge regions enhances the occurrence frequency of IC discharges than CG discharges, which brings the enhancement of the *Z*-ratio.

3.4 Latitudinal Dependence of *Z*-ratio

The zonal-mean *Z*-ratio was calculated, and its latitudinal dependences in the northern and southern hemispheres are plotted in Figures 8(a) and 8(b), respectively. The vertical bars attached to each data point represent the standard deviation (±1σ level) of the *Z*-ratio variation in each latitudinal range. It is found that the *Z*-ratio gradually decreases from the equator to the higher latitude from 2.9 to 0.2 in the northern hemisphere as shown in Figure 8(a), while from 2.9 to 0.5 in the southern hemisphere as shown in Figure 8(b). These characteristics are well comparable to the results reported by Pierce (1970), Prentice and Mackerras (1977), Mackerras and Darveniza (1994), Mackerras et al. (1998), and Boccippio et al. (2001). The comparison between the *Z*-ratios derived from this study and previous studies are summarized in Table 2. As shown in this table, the mean value of the *Z*-ratio, which is shown in the bracket in the latitudinal range of 20ºS-20ºN, is estimated to be 2.5 with a standard deviation of 0.46. This value is smaller than the tropical (20ºS-20ºN) *Z*-ratio (6.2 and 5.9) estimated by Pierce (1970) and Prentice and Mackerras (1977), while this value well agrees with the *Z*-ratio estimated by Mackerras and Darveniza (1994), where the mean *Z*-ratio in the tropics was 2.3. At the latitudinal range of 20ºN - 40ºN and 20ºS - 40ºS, the mean value of *Z*-ratio is 1.9 with a standard deviation 0.33, again it is considerably lower than the ratio of 4.2 by Prentice and Mackerras, (1977) and 2.2 by Mackerras and Darveniza (1994) in the same latitudinal range. As for the result of the *Z*-ratio in the latitudinal range of 40ºN - 60ºN and 40ºS - 60ºS, the mean *Z*-ratio value derived from this study is 1.1. It is lower than the ratio of 1.3 by Mackerras and Darveniza

(1994) in this latitudinal range. There are two possible explanations for this disagreement. First, there were limitations of the visual and flash counter observations in the previous studies. The obtained results were not reliable in the high lightning activity regions because of the difficulty in distinguishing between IC and CG discharges. Second, there were limitations of the observation areas. In the previous studies, *Z*-ratios were estimated from the lightning data obtained over the land region, and they did not include the ratios over the oceanic areas where the *Z*-ratios are believed to have lower values than those over land regions as we presented in Section 3.1.

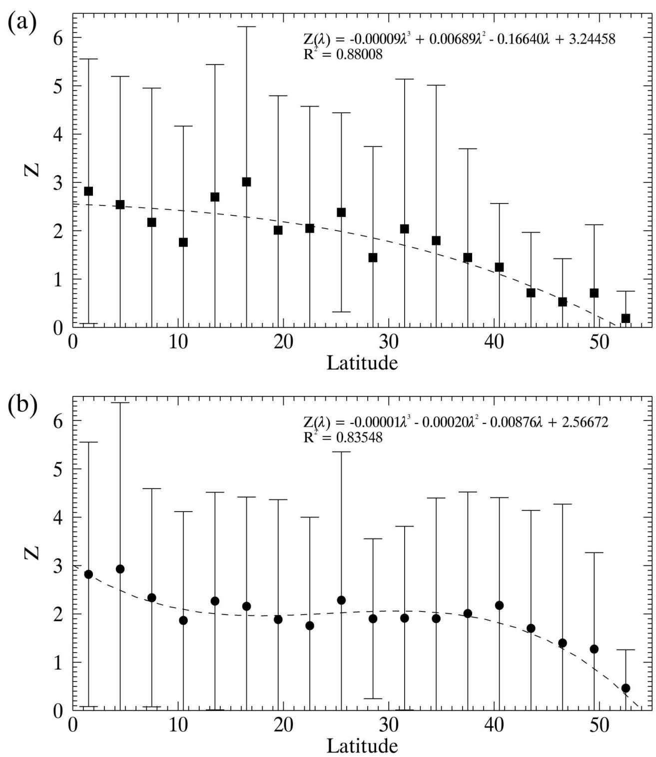

Figure 8. (a) Latitudinal dependences of the *Z*-ratio in the northern hemisphere. (b) Same as (a) except for the southern hemisphere. In these figures, the zonal-mean *Z*-ratio values are calculated every 3° latitudinal range and plotted. Vertical bars at each data point represent the ±1σ of Z-ratio values in the corresponding 3° latitudinal range.

Table 2. Comparison between the *Z*-ratios derived from this study and the previous studies.

	This study	Pierce, 1970	Prentice and Mackerras, 1977	Soriano and de Pablo, 2007	Mackerras and Darveniza, 1994
Coverage	50°S - 50°N	–	–	50°S - 50°N	50°S - 50°N
20°S - 20°N	2.9 - 1.7 (2.5)	9.0 - 4.4 (6.2)	6.3 - 5.2 (5.9)	–	3.4 - 0.5 (2.3)
20°N - 40°N, 20°S - 40°S	2.4 - 1.2 (1.9)	4.4 - 2.8 (3.5)	5.2 - 3.1 (4.2)	6.1 - 2.2 (3.5)	3.8 - 1.1 (2.2)
40°N - 60°N, 40°S - 60°S	1.9 - 0.19 (1.1)*	2.8 - 2.2 (2.5)	3.1 - 2.0 (2.4)		1.5 - 1.0 (1.3)

* latitudinal range = 40°N - 51°N and 40°S - 51°S

The relation between the occurrence ratio (%) of IC, -CG, and +CG discharges and *Z*-ratio at each 3.0°×3.0° grid is plotted in Figure 9. In Figure 9(a), each data point shows the pairwise value of the Z-ratio and the percentage of IC discharges for each 3.0°×3.0° grid block. The Z-ratio in this plot is the corresponding to Figure 6. Figure 9(b) and 9(c) same as 9(a) except for +CG and -CG discharges, respectively. Prior studies have reported a significant relationship between *Z*-ratio and +CG discharges. The high *Z*-ratio values tend to appear in the regions where the occurrence percentage of +CG discharges is high (Boccippio et al., 2001; Pinto et al., 2003; Soriano and de Pablo, 2007). In this study, however, we found that the occurrence percentage of +CG discahrges decreases when the *Z*-ratio increases as shown in Figure 9(b). We also found clear relations between the increasing *Z*-ratio and the increasing occurrence percentage of IC discharges (Figure 9(a)) and between the decreasing *Z*-ratio and the increasing occurrence percentage of -CG discharges (Figure 9(c)).

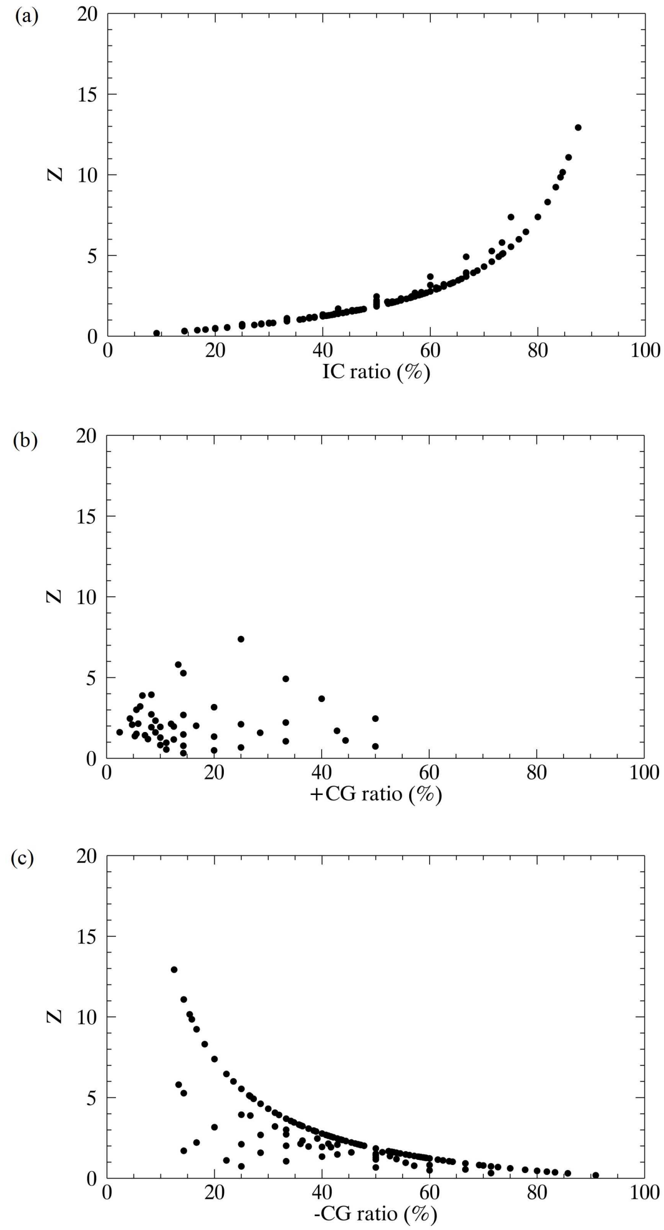

Figure 9. Scatter plot of the estimated *Z*-ratio toward the occurrence percentage of (a) IC, (b) +CG, and (c) -CG discharges, respectively.

4. Conclusion

The occurrence ratio of IC discharges to CG discharges (*Z*-ratio) was estimated using the lightning optical data obtained by the JEM-GLIMS mission in the period from November 2012 to August 2015. The results derived from our analysis show that the *Z*-ratio in the continental thunderclouds is higher than that of the oceanic thunderclouds, especially in the area where the lightning activities are high, *i.e.*, central Africa, south-east Asia, and central America. It is also found that the *Z*-ratio in the local summer season is higher than that in the local winter season. The latitudinal dependence of the *Z*-ratio is clearly found, which is comparable to the previous studies (Pierce, 1970; Prentice and Mackerras, 1977; Mackerras et al., 1998). The estimated *Z*-ratio varies from 2.9 - 0.19 from the tropics (20°S - 20°N) to the mid-latitude (20°S - 40°S and 20°N - 40°N) with the global mean of 1.6. The decrease of the *Z*-ratio from the tropics to the mid-latitude is confirmed both in the northern and southern hemispheres. This present finding is useful to quantitatively estimate the occurrence number of IC discharges by combining to the ground-based lightning data, such as WWLLN, which we currently proceed in the development of the three-dimensional global electrical circuit (GEC) model in order to investigate the contribution of global lightning activities to GEC as the electrical generator.

Appendix A.

Lightning Detection Efficiency of JEM-GLIMS

As we mentioned in section 2, the JEM-GLIMS optical instruments were designed to detect optical emissions of lightning discharges and lightning-associated TLEs. The event triggering threshold of these instruments was set to be high due to the limitation of the telemetry speed between the ISS and the ground, and the average detection number was ~10 events/day. Therefore, JEM-GLIMS optical instruments detected only intense lightning emissions and missed many weak lightning emissions, that tend to have smaller optical energy. Figure 10 shows the optical energy distribution of JEM-GLIMS lightning events measured in the period from November 2012 to August 2015. Each data point shows the optical energy in the wavelength range of 400 - 1000 nm which was calculated from PH4(599-900 nm) lightning curve data. The optical energy in the wavelength range of 599 - 900 nm is 29.2% of the optical energy radiated by lightning discharges in the wavelength range of 400 - 1000 nm (Orville and Henderson, 1984). Therefore, we also included this percentage in the calculation of the optical energy in the wavelength range of 400 - 1000 nm for all JEM-GLIMS lightning flashes. It is found that these events have the optical energy larger than 2.1×10^6 J. This means that the JEM-GLIMS optical instruments missed lightning flashes having the optical energy less than 2.1×10^6 J. In order to estimate the JEM-GLIMS detection efficiency of lightning emissions, *i.e.*, the ratio between detected lightning events and total lightning events, we first performed further analysis to classify the relation between the optical energy of lightning discharges and the detection number of lightning discharges. Figure 11 shows the relation between the detection number of lightning discharges by the JEM-GLIMS optical instruments and optical energy. For this plot, the optical energy of each data point was estimated every 0.001 MJ step. Then, we use the linear regression to find the correlation between the occurrence number and the optical energy in the optical energy range from 0.08×10^6 J to 102.0×10^6 J, as shown by the solid and dashed lines in Figure 11. The reason why we used this optical energy range is that the average optical energy of IC, +CG, and -CG discharges are 1.5×10^6 J, 9.7×10^6 J, and 3.5×10^6 J, respectively, and that these numbers well agree with the optical energies reported by the earlier studies (Orville, 1980; Orville and Henderson, 1984; Quick and Krider, 2013). We found the correlation between the occurrence number of IC, +CG, and -CG discharges, and the occurrence number of lightning discharges can be empirically estimated by the following linear regression functions,

$$N_{IC}(E) = -336.1 \ln(E) + 1352 \qquad (2)$$

$$N_{+CG}(E) = -12.21 \ln(E) + 69.53 \qquad (3)$$

$$N_{-CG}(E) = -89.15 \ln(E) + 417.4 \qquad (4)$$

where $N_{IC}(E)$, $N_{+CG}(E)$, and $N_{-CG}(E)$ are the occurrence number of IC, +CG, and -CG discharges having the optical energy of E, respectively. Then, the total occurrence number of IC, +CG, -CG discharges, *i.e.*, (N_{IC}, N_{+CG}, N_{-CG}), can be estimated by integrating the equations (2), (3), and (4) in the energy range from 0.08×10^6 J to 102.0×10^6 J. Finally, the detection efficiency (DE) is estimated by

$$DE_{IC} = 100 \times N_{IC\,glims} / N_{IC} \qquad (5)$$

$$DE_{+CG} = 100 \times N_{+CG\,glims} / N_{+CG} \qquad (6)$$

$$DE_{-CG} = 100 \times N_{-CG\,glims} / N_{-CG} \qquad (7)$$

where $N_{IC\ glims}$, $N_{+CG\ glims}$, and $N_{-CG\ glims}$ are the number of IC, +CG, and -CG discharges detected by JEM-GLIMS optical instruments. Using this method, the JEM-GLIMS detection efficiency of IC, +CG, and -CG discharges are estimated to be 11.2%, 28.3%, and 19.7%, respectively.

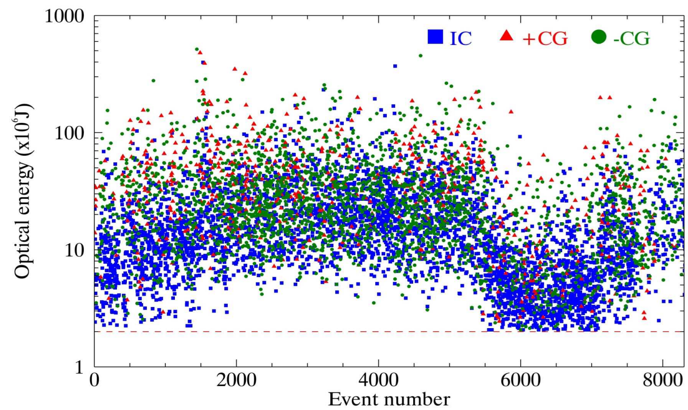

Figure 10. Optical energy distribution of lightning events detected by JEM-GLIMS optical instruments in the wavelength range of 400 - 1000 nm.

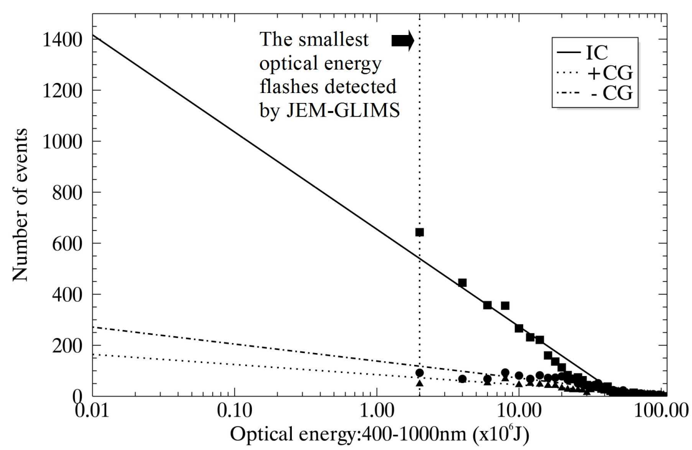

Figure 11. Relationship between the number of lightning events and the optical energy in the wavelengths 400 - 1000 nm. The solid and dashed lines are the linear regression functions.

Acknowledgments

This work was supported by JSPS KAKENHI Grant-in-Aid for Scientific Research (B) Number 16H04055 and 24340117, and MEXT KAKENHI Grant-in-Aid for Specially Promoted Research Number 19002002. The authors wish to thank the World Wide Lightning Location Network (http://wwlln.net), a collaboration among over 50 universities and institutions, for providing the lightning location data used in this paper. The lightning data over Japan and North America was provided by the Franklin Japan Corporation (https://www.franklinjapan.jp) and Vaisala's National Lightning Detection Network (https://www.vaisala.com), respectively. The global ELF data in this study can be requested from the Global ELF Observation Network (http://www.ep.sci.hokudai.ac.jp/~geon/). The JEM-GLIMS lightning data used in this study can be requested from the websites http://www.ep.sci.hokudai.ac.jp/~jemglims. Additional related files can be found at .... All data analyses and figures in this work were performed using the Interactive Data Language (IDL 8.2).

References

Adachi, T., M. Sato, T. Ushio, A. Yamazaki, M. Suzuki, M. Kikuchi, Y. Takahashi, U. Inan, I. Linscott, Y. Hobara, H. U. Frey, S. B. Mende, A. B. Chen, R. Hsu, and K. Kusunoki (2016), Identifying the occurrence of lightning and transient luminous events by nadir spectrophotometric observation, *J. Atmos. Solar-Terr. Phys.*, 145, 85–97, doi:10.1016/j.jastp.2016.04.010.

Ballarotti, M. G., M. M. F. Saba, and O. Pinto Jr. (2005), High-speed camera observations of negative ground flashes on a millisecond-scale, *Geophys. Res. Lett.,* 32*,* L23802, doi:10.1029/2005GL023889.

Bandholnopparat, K., M. Sato, Y. Takahashi, T. Adachi, and T. Ushio (2017), Estimation of the IC to CG ratio using JEM-GLIMS and ground-based lightning network data, *AGU Fall Meeting 2017*, AE33A-2520, New Orleans, USA, December 2017.

Bandholnopparat, K., M. Sato, T. Adachi, T. Ushio, and Y. Takahashi (2019), Optical properties of intracloud and cloud-to-ground discharges derived from JEM-GLIMS lightning observations, *J. Atmos. Solar-Terr. Phys.*, 189, 87-97, doi:10.1016/j.jastp.2019.04.005.

Boccippio, D. J., W. Koshak, R. Blakeslee, K. Driscoll, D. Mach, D. Buechler, W. Boeck, H. J. Christian, and S. J. Goodman (2000), The Optical Transient Detector (OTD): Instrument characteristics and cross-sensor validation, *J. Atmos. Ocean. Tech.*, 17(4), 441–458. doi:10.1175/1520-0426(2000)017<0441:TOTDOI>2.0.CO;2.

Boccippio, D. J., K. L. Cummins, H. J. Christian, and S. J. Goodman (2001), Combined satellite- and surface-based estimation of the intracloud–cloud-to-ground lightning ratio over the continental United States, *Month. Weath. Rev.*, 129(1), 108–122, doi:10.1175/1520-0493(2001)129<0108:CSASBE>2.0.CO;2.

Buechler, D. E., K. T. Driscoll, S. J. Goodman, and H. J. Christian (2000), Lightning activity within a tornadic thunderstorm observed by the optical transient detector (OTD), *Geophys. Res. Lett.*, 27(15), 2253–2256, doi:10.1029/2000GL011579.

Christian, H. J., et al. (2003), Global frequency and distribution of lightning as observed from space by the Optical Transient Detector, *J. Geophys. Res. - Atmos.*, 108(D1), 4005, doi:10.1029/2002JD002347.

de Souza, P. E., O. Pinto, I. R. C. A. Pinto, N. J. Ferreira, and A. F. dos Santos (2009), The intracloud/cloud-to-ground lightning ratio in Southeastern Brazil, *Atmos. Res.*, 91, 491–499. doi:10.1016/j.atmosres.2008.06.011.

Hutchins, M. L., R. H. Holzworth, J. B. Brundell, and C. J. Rodger (2012), Relative detection efficiency of the World Wide Lightning Location Network, *Radio Sci.*, 47, RS600, doi:10.1029/2012RS005049.

Koshak, W. J., R. J. Solakiewicz, D. D. Phanord, and R. J. Blakeslee (1994), Diffusion model for lightning radiative transfer, *J. Geophys. Res. - Atmos.,* 99(D7), 14361–14371, doi:10.1029/94JD00022.

Koshak, W. J. (2010), Optical characteristics of OTD flashes and the implications for flash-type discrimination, *J. Atmos. Ocean. Tech.*, 27(11), 1822–1838. doi:10.1175/2010JTECHA1405.1.

Kuleshov, Y., D. Mackerras, and M. Darveniza (2006), Spatial distribution and frequency of lightning activity and lightning flash density maps for Australia, *J. Geophys. Res.- Atmos.*, 111, D19105, doi:10.1029/2005JD006982.

Lhermitte, R., and E. Williams (1983), Cloud electrification, *Rev. Geophys.,* 21*,* 984–992, doi:10.1029/RG021i005p00984.

López, J. A., J. Montanyà, O. Van Der Velde, D. Romero, H. Aranguren, H. Torres, J. Taborda, and J. Martinez (2016), First data of the Colombia lightning mapping array - COLMA. *Proceeding of the 33rd International Conference on Lightning Protection, ICLP 2016*, Estoril, Portugal, do:10.1109/ICLP.2016.7791436.

Lu, G., S. A. Cummer, R. J. Blakeslee, S. Weiss, and W. H. Beasley (2012), Lightning morphology and impulse charge moment change of high peak current negative strokes, *J. Geophys. Res. - Atmos.*, 117(D4), D04212, doi:10.1029/2011JD016890.

Lyu, F., S. A. Cummer, G. Lu, X. Zhou, and J. Weinert (2016), Imaging lightning intracloud initial stepped leaders by low-frequency interferometric lightning mapping array, *Geophys. Res. Lett.,* 43, 5516–5523, doi:10.1002/2016GL069267.

Mackerras, D. (1968), A comparison of discharge processes in cloud and ground lightning flashes, *J. Geophys. Res.,* 73, 1175-1183, doi:10.1029/JB073i004p01175.

Mackerras, D., and M. Darveniza (1994), Latitudinal variation of lightning occurrence characteristics, *J. Geophys. Res. - Atmos.,* 99(D5), 10813–10821, doi:10.1029/94JD00018.

Mackerras, D., M. Darveniza, R. E. Orville, E. R. Williams, and S. J. Goodman (1998), Global lightning: Total, cloud and ground flash estimates, *J. Geophys. Res. - Atmos.,* 103(D16), 19791-19809, doi:10.1029/98JD01461.

Mareev, E. A., and E. M. Volodin (2014), Variation of the global electric circuit and Ionospheric potential in a general circulation model, *Geophys. Res. Lett.*, 41(24), 9009–9016, doi:10.1002/2014GL062352.

Mecikalski, R. M., and L. D. Carey (2018), Radar reflectivity and altitude distributions of lightning as a function of IC, CG, and HY flashes: Implications for LNOx production, *J. Geophys. Res. - Atmos.,* 123, 12796–12813, do:10.1029/2018JD029238.

Norville, K., M. Baker, and J. Latham (1991), A numerical study of thunderstorm electrification: Model development and case study, *J. Geophys. Res., 96 (D4)*, 7463–7481.

Orville, R. E. (1980), Daylight spectra of individual lightning flashes in the 370–690 nm region, *J. App. Meteorol.,* 19, 470-473, doi:10.1175/1520-0450(1980)019<0470:DSOILF>2.0.CO;2.

Orville, R. E., and R. W. Henderson (1984), Absolute spectral irradiance measurements of lightning from 375 to 880 nm, *J. Atmos. Sci.,* doi:10.1175/1520-0469(1984)041<3180:ASIMOL>2.0.CO;2.

Ott, L. E., K. E. Pickering, G. L. Stenchikov, D. J. Allen, A. J. DeCaria, B. Ridley, R. F. Lin, S. Lang, and W. K. Tao (2010), Production of lightning NOx and its vertical distribution calculated from three-dimensional cloud-scale chemical transport model simulations, *J. Geophys. Res. - Atmos.*, 115(D4), D04301. doi:10.1029/2009JD011880.

Pawar, S. D., and A. K. Kamra (2004), Evolution of lightning and the possible initiation/triggering of lightning discharges by the lower positive charge center in an isolated thundercloud in the tropics, *J. Geophys. Res. - Atmos.,* 109(D2), D02205, doi:10.1029/2003JD003735.

Pickering, K.E., Y. Wang, W. K. Tao, C. Price, and J. F. Müller (1998), Vertical distributions of lightning NOx for use in regional and global chemical transport models, *J. Geophys. Res. - Atmos.*, 103, 31203–31216, doi:10.1029/98JD02651.

Pierce, E. T. (1970), Latitudinal variation of lightning parameters, *J. App. Meteorol.*, 9, 194-195, doi:10.1175/1520-0450(1970)009<0194:LVOLP>2.0.CO;2.

Pinto, O.Jr., I. R. C. A. Pinto, J. H. Diniz, A. Cazetta Filho, L. C. L. Chechiglia, and A. M. Carvalho (2003), A seven-year study about the negative cloud-to-ground lightning flash characteristics in Southeastern Brazil, *J. Atmos. Solar-Terr. Phys.,* 65, 739–748, doi:10.1016/S1364-6826(03)00077-4.

Prentice, S. A., and D. Mackerras (1977), The ratio of cloud to cloud-ground lightning flashes in thunderstorms, *J. App. Meteorol.,* 16, 545-550, doi:10.1175/1520-0450(1977)016<0545:TROCTC>2.0.CO;2.

Quick, M. G., and E. P. Krider (2013), Optical power and energy radiated by natural lightning, *J. Geophys. Res. - Atmos.*, 118(4), 1868–1879, doi:10.1002/jgrd.50182.

Rakov, V. A., and M. A. Uman (2003), Lightning: Physics and effect (encyclopedia of lightning). *Cambridge University Press, ISBN 0521583276, Chapter 2, 24-66,* London, England.

Rodger, C. J., S. Werner, J. B. Brundell, E. H. Lay, N. R. Thomson, R. H. Holzworth, and R. L. Dowden (2006), Detection efficiency of the VLF World-Wide Lightning Location Network (WWLLN): Initial case study, *Ann. Geophys.*, 24(12), 3197–3214, doi:10.5194/angeo-24-3197-2006.

Rodger, C J., J. B. Brundell, R. H. Holzworth, and E.H. Lay (2009), Growing detection efficiency of the World Wide Lightning Location Network, *AIP Conf. Proc.,* 1118, doi:10.1063/1.3137706.

Rust, W. D., D. R. MacGorman, and R. T. Arnold (1981), Positive cloud-to-ground lightning flashes in severe storms, *Geophys. Res. Lett.*, 8(7), 791– 794, doi:10.1029/GL008i007p00791.

Rycroft, M. J., and A. Odzimek (2010), Effects of lightning and sprites on the ionospheric potential, and threshold effects on sprite initiation, obtained using an analog model of the global atmospheric electric circuit, *J. Geophys. Res. - Space Phys.*, 115(A6), A00E37, doi:10.1029/2009JA014758.

Sato, M., H. Fukunishi, M. Kikuchi, H. Yamagishi, and W. A. Lyons (2003), Validation of sprite-inducing cloud-to-ground lightning based on ELF observations at Syowa station in Antarctica, *J. Atmos. Solar-Terr. Phys.*, 65(5), 607–614, doi:10.1016/S1364-6826(02)00327-9.

Sato, M., Y. Takahashi, M. Suzuki, A. Yamazaki, and T. Ushio (2011a), Six-channel spectrophotometers(PH) onboard JEM-GLIMS. *IEEJ Trans. F. M.,* 131(12)*,* 1000-1005, doi:10.1541/ieejfms.131.1000.

Sato, M., Y. Takahashi, M. Kikuchi, M. Suzuki, A. Yamazaki, and T. Ushio (2011b), Lightning and Sprite Imager (LSI) on board JEM-GLIMS, *IEEJ Trans. F. M.,* 131(112), 994-999, doi:10.1541/ieejfms.131.994.

Sato, M., et al. (2015), Overview and early results of the Global Lightning and Sprite Measurements mission, *J. Geophys. Res. - Atmos.*, 120, 3822–3851, doi:10.1002/2014JD022428.

Sato M., et al. (2016), Horizontal distributions of sprites derived from the JEM-GLIMS, *J. Geophys. Res. - Atmos.*, 121, 3171-3194, doi:10.1002/2015JD024311.

Soriano, L. R., and F. de Pablo (2007), Total flash density and the intracloud/cloud-to-ground lightning ratio over the Iberian Peninsula, *J. Geophys. Res. - Atmos.,* 112(D13), D13114, doi:10.1029/2006JD007624.

Stolzenburg, M., Rust, W. D., Smull, B. F., and T. C. Marshall (1998a), Electrical structure in thunderstorm convective regions: 1. Mesoscale convective systems, *J. Geophys. Res. - Atmos.*, 103(D12), 14059–14078, doi:10.1029/97JD03546.

Stolzenburg, M., Rust, W. D., and T. C. Marshall (1998b), Electrical structure in thunderstorm convective regions: 2. Isolated storms, *J. Geophys. Res. - Atmos.*, 103(D12), 14079–14096, doi: 10.1029/97JD03547.

Stolzenburg, M., Rust, W. D., and T. C. Marshall (1998c), Electrical structure in thunderstorm convective regions: 3. Synthesis, *J. Geophys. Res. - Atmos.*, 103(D12), 14097–14108, doi: 10.1029/97JD03545.

Stolzenburg, M., T. C. Marshall, S. Karunarathne, N. Karunarathna, L. E. Vickers, T. A. Warner, R. E. Orville, and H.-D. Betz (2013), Luminosity of initial breakdown in lightning, *J. Geophys. Res. - Atmos*., 118, 2918–2937, doi:10.1002/jgrd.50276.

Sun, Z., X. Qie, M. Liu, R. Jiang, Z. Wang, and H. Zhang (2016), Characteristics of a negative lightning with multiple-ground terminations observed by a VHF lightning location system, *J. Geophys. Res. - Atmos.,*121, 413–426, doi:10.1002/2015JD023702.

Takahashi, T. (1984), Thunderstorm electrification - A numerical study, *J. Atmos. Sci.,* 41, 2541–2558, doi:10.1175/1520-0469(1984)041<2541:TENS>2.0.CO;2.

Ushio, T., M. Sat, T., Morimoto, H. Kikuchi, M., Suzuki, A. Yamazaki, Y. Hobara, M. Kikuchi, U. Inan, I. Linscott, H. Kikuchi, R. Ishida, Y. Takahashi, and T. Adachi (2014), Global lightning and sprite measurements from International Space Station, *Proceeding at the*

31th URSI General Assembly and Scientific Symposium, Oklahoma, USA, doi:10.1109/URSIGASS.2014.6929579.

Williams, E., B. Boldi, A. Matlin, M. Weber, S. Hodanish, D. Sharp, S. D. Goodman, R. Raghavan, and D. Buechler (1999), The behavior of total lightning activity in severe Florida thunderstorms, *Atmos. Res.*, 51(3-4), 245–265, doi:10.1016/S0169-8095(99)00011-3.

Williams, E. R. (2009), The global electrical circuit: A review, *Atmos. Res.*, 91(2-4), 140-152, doi:10.1016/j.atmosres.2008.05.018.

Ziegler, C. L., D. R. MacGorman, J. E. Dye, and P. S. Ray (1991), A model evaluation of noninductive graupel-ice charging in the early electrification of a mountain thunderstorm, *J. Geophys. Res. - Atmos.,* 96(D7)*,* 12833– 12855, doi:10.1029/91JD01246.

Zipser E. J. (1994), Deep cumulonimbus cloud systems in the tropics with and without lightning, *Mon. Wea. Rev.,* 122, 1837-1851, doi:10.1175/1520-0493(1994)122<1837:DCCSIT>2.0.CO;2.

Zipser E. J. and K. R. Lutz (1994), The vertical profile of radar reflectivity of convective cells: A strong indicator of storm intensity and lightning probability?, *Mon. Wea. Rev.,* 122*,* 1751–1759, doi:10.1175/1520-0493(1994)122<175:TVPORR>2.0.CO;2.